Analysis of Climate Change Projections for the Okavango River Basin

Authors:
T. Weber, A. Kriegsmann, B. Eggert and D. Jacob
Climate Service Center 2.0
Helmholtz-Zentrum Geesthacht
Fischertwiete 1
20095 Hamburg
Germany

These results were created in the project "The Future Okavango" (TFO) founded by the German Federal Ministry of Education and Research.

For the TFO-scenario building process, the climate change scenarios are of uppermost interest, because the potential change of the climate in the Okavango River Basin may affect all components of the hydrological cycle, and thus the lives of the people living this region. In order to develop strategies for sustainable land management in the basin, scientists from various disciplines and decision makers need high resolution climate change information. To generate high resolution climate projections, regional climate models are used to downscale simulations created by global circulation models. Climate projections, however, contain various uncertainties which have to be considered and estimated. The uncertainty originating from climate models can be estimated by applying different global circulation models and regional climate models. In long-term climate change projections, however, the largest portion of uncertainty is assigned to the human contribution to climate change, which is a result of unknown developments in technology, economies, lifestyle and policy. This uncertainty can be tackled using different emission scenarios covering a wide range of possible future anthropogenic emissions. In the TFO project the new Representative Concentrations Pathways (RCPs) are considered, which contain a possible moderate (RCP4.5) and a high (RCP8.5) anthropogenic emission scenario (Moss et al., 2010). Thereby, the numbers 4.5 and 8.5, respectively, indicate the additional radiative forcing in W/m² of the atmosphere by the end of the 21st century. Finally, the uncertainty resulting from the climate variability can be reduced by considering a sufficiently long period of time such as a 30-years mean of a meteorological variable.

In TFO, subproject 01 generated future climate change projections at a high spatial resolution for the Okavango River Basin. The regional climate change projections were dynamically downscaled with the regional climate model REMO (Jacob, 2001) using data from the global circulation models ECHAM6 (Stevens et al., 2015) and EC-EARTH (Hazeleger et al., 2010) as forcing. To obtain the high spatial resolution of 25 x 25 km² of the regional climate change projections, a double nesting method was applied. The climate change signals were analysed for a near-future (2016-2045) and a far-future (2071-2100) period, and respective to the reference period 1971-2000. The rate of change for each meteorological variable is indicated by a bandwidth, which expresses the uncertainty resulting from the two different emission scenarios and the global model forcings.

For the trend analysis, the Okavango River Basin is divided into three sub-domains which accounts for the diverse topography and climate along the river (Fig. 1). Sub-domain 1 (SD1) (lon.: 15.75 °E to 19.71 °E, lat.: 15.49 °S to 12.19 °S) covers the northern part of the basin with the Angolan highlands being the source region of the Okavango River. Sub-domain 2 (SD2) (lon.: 16.63 °E to 21.69 °E, lat.: 17.91 °S to 15.49 °S) contains the down streams areas of the river between the Angolan highlands and the Angolan/Namibian border, and Sub-domain 3 (SD 3) (lon.: 16.19 °E to 28.51 °E, lat.: 25.17 °S to 17.91 °S) encompasses the southern part of the basin with the Okavango Delta and the Kalahari Desert.

Extreme events in daily precipitation are estimated using the 95th percentile of daily precipitation intensity and its occurrence. The duration of the rainy season was calculated based on the definition by Liebmann et al. (2012), and the dry spells during the rainy seasons are determined by the number of periods in the rainy season with at least six consecutive days with daily rain amounts of less than 1 mm per day.

Temperature

Projected Trend

The climate change projections show an increase in annual mean temperature for all three sub-domains throughout of the century. Thereby the low emission scenario simulation (RCP4.5) shows a moderate increase and the high emission scenario simulation (RCP8.5) a strong increase in temperature (Fig. 2a-c).

For the near-future (2016-2045), the annual mean temperature is projected to increase with a total range for SD1 between 1.2 °C and 1.7 °C (Fig. 2a), for SD2 between 1.3 °C and 2.0 °C (Fig. 2b) and for SD3 between 1.2 °C and 1.8 °C (Fig. 2c) respective to 1971-2000. Considering the two emission scenarios separately, the RCP4.5 scenario simulation suggests an increase in annual mean temperature for SD1 between 1.2 °C and 1.4 °C (Fig. 2a), for SD2 between 1.3 °C and 1.6 °C (Fig. 2b) and for SD3 between 1.2 °C and 1.6 °C (Fig. 2c). The RCP8.5 scenario simulation suggests for SD1 between 1.6 °C and 1.7 °C (Fig. 2a), for SD2 between 1.8 °C and 2.0 °C (Fig. 2b) and for SD3 between 1.5 °C to 1.8 °C respectively (Fig. 2c).

For far-future period, the model simulates an increase in annual mean temperature with a total range for SD1 between 2.4 °C and 5.2 °C (Fig. 2a), for SD2 between 2.2 °C and 5.8 °C (Fig. 2b) and for SD3 between 2.4 °C and 5.7 °C (Fig. 2c) related to 1971-2000. Looking at the two emission scenarios separately, the RCP4.5 scenario simulation indicates an increase in annual mean temperature for SD1 between 2.4 °C and 2.5 °C (Fig. 2a), for SD2 between 2.2 °C and 2.8 °C (Fig. 2b) and for SD3 between 2.4 °C and 2.6 °C (Fig. 2c). The RCP8.5 scenario simulation indicates for SD1 between 4.8 °C and 5.2 °C (Fig. 2a), for SD2 between 5.4 °C and 5.8 °C (Fig. 2b) and for SD3 between 4.9 °C and 5.7 °C respectively (Fig. 2c).

Spatial distribution of projected change

For the near-future (2016-2045), the southern Angolan and the Namibian part of the Okavango River Basin and the Okavango River Delta are expected to experience a more intense warming of 1.0 °C to 2.0 °C under the RCP4.5 (Fig. 3a/c) and of 1.5 °C to 2.5 °C under the RCP8.5 scenario (Fig. 3b/d) than the other areas respective to 1971-2000. For the far-future (2071-2100), a stronger increase in annual mean temperature for this area is projected with 2.0 °C to 3.0 °C under the RCP4.5 respectively (Fig. 4a/c) and with 5.0 °C to 6.5 °C under the RCP8.5 scenario (Fig. 4b/d). The warming patterns seem to be a result of the topography in the basin and of the influence of the Kalahari Desert.

The mean minimum temperature in the wet season (Dec.-Feb.) is expected to rise, in particular, in the southern Angolan and Namibian/Botswanan part of the basin for the near-future (2016-2045). Both emission scenarios project an increase between 1.0 °C and 2.0 °C (Fig. 5a/b/c/d) respective to 1971-2000. In the dry season (Jun.-Aug.), the warming area is spreading from the southeastern part of the basin to the Angolan highlands with 1.0 °C to 2.0 °C under the RCP4.5 (Fig. 6a/c) and with 1.0 °C to 2.5 °C under the RCP8.5 scenario (Fig. 6b/d) under the same period. For the far-future (2071-2100), the mean minimum temperature in the wet season (Dec.-Feb.) is expected to increase southerly of the Angolan highlands between 1.5 °C and 3.0 °C under the RCP4.5

(Fig. 7a/c), and between 4.0 °C and 7.0 °C with a hotspot in the Okavango River Delta under the RCP8.5 scenario (Fig. 7b/d). In the dry season (Jun.-Aug.), the model simulates a rise of the mean minimum temperature in an area from the Okavango River Delta to the northern part of the basin with 1.5 ° to 3.0 °C under the RCP4.5 (Fig. 8a/c) and with 4.0 °C to 6.0 °C under the RCP8.5 scenario (Fig. 8b/d).

The mean maximum temperature is projected to increase in the wet season (Dec.-Feb.) for an area covering the Okavango River Delta, the Namibian part and the southern Angolan part of the basin for the near-future (2015-2046).The model simulates an increase of 0.5 °C to 2.0 °C under the RCP4.5 (Fig. 9a/c) and of 1.0 °C to 2.5 °C in the uppermost eastern and in the western part of the basin under the RCP8.5 scenario respectively (Fig. 9b/d). In the dry season (Jun.-Aug.), the mean maximum temperature is projected to rise of 1.0 °C to 2.5 °C for an area from the Okavango River Delta to the northern part of the basin under the RCP4.5 (Fig. 10a/c) and of 1.0 °C to 3.0 °C under the RCP8.5 scenario simulation respectively (Fig. 10b/d) for the same period. For the far-future (2071-2100), the projections of the mean maximum temperature in the wet season (Dec.-Feb.) show an increase of 2.0 °C to 3.5 °C in an area from the Okavango River Delta to the Angolan highlands under RCP4.5 (Fig.11a/c), and an increase of 4.0 °C to 7.0 °C in the basin southerly of the Angolan highlands under the RCP8.5 scenario (Fig.11b/d). In the dry season (Jun.-Aug.), the model simulates a rise of the mean maximum temperature for an area from the Okavango River Delta to the northern part of the basin. The increase is projected with 2.0 °C to 3.5 °C under the RCP4.5 (Fig.12a/c) and with 5.0 °C to 7.0 °C in the Okavango River Delta, the Namibian and Angolan part of the basin under the RCP8.5 scenario respectively (Fig. 12b/d).

Precipitation

Projected Trend

The model simulates for all sub-domains a decline in mean daily precipitation with a high interannual variation throughout the century. While the RCP4.5 scenario simulation shows a small reduction in mean daily precipitation in all sub-domains, the RCP8.5 shows a medium (north) to strong (south) reduction (Fig. 13.a-c). However, it has to be mentioned that the annual precipitation in the southernmost SD3 is much lower compared to the one in the northernmost SD1.

For the near-future (2016-2045), the climate change projections indicate a decline in mean daily precipitation with a total range for SD1 between -9 % and -1 % (Fig. 13a), for SD2 between -11 % and -5 % (Fig.13b) and for SD3 between -11 % and -3 % (Fig. 13c) respective to 1971-2000. Considering the two emission scenarios separately, the RCP4.5 scenario suggests a reduction in mean daily precipitation for SD1 between -5 % and -1 % (Fig. 13a), for SD2 of about -5 % (Fig. 13b) and for SD3 between -7 % and -3 % (Fig. 13c). The RCP8.5 scenario simulation projects for SD1 between -9 % and -6 % (Fig. 13a), for SD2 and SD3 between -11 % and -8 % respectively (Fig. 13b/c).

For far-future period, the models project a decline in mean daily precipitation with a total range for SD1 between -13 % and -3 % (Fig. 13a), for SD2 between -24 % and -6 % (Fig.13b) and for SD3 between -32 % and -6 % (Fig.13c) respective to 1971-2000. Looking at the two emission scenarios separately, the RCP4.5 scenario simulation shows reduction in mean daily precipitation for SD1 between -7 % and -3 % (Fig.13a), for SD2 between -9 % and -6 % (Fig.13b) and for SD3 between -11 % and -6 % (Fig. 13c). The RCP8.5 scenario simulation projects for SD1 between -13 % and -9 % (Fig.13a), for SD2 between -24 % and -23 % (Fig.13b) and for SD3 between -32 % and -24 % respectively (Fig.13c).

Spatial distribution of projected change

For the near-future (2016-2045), the mean daily precipitation during the wet season (Dec.-Feb.) shows a change between -1.5 mm and 1 mm over the whole Okavango River Basin with a tendency for a reduction in the northern Angolan part and northern Botswanan part under the RCP4.5 scenario simulation respective to 1971-2000 (Fig. 14a/c). The model projects a reduction between -2 mm and 0 mm in the Angolan/Namibian and northern Botswanan part of the basin under the RCP8.5 scenario simulation (Fig. 14b/d). For the far-future (2071-2100), the projections indicate change in mean daily precipitation between -1.5 mm and 1.0 mm over the whole basin under the RCP4.5 scenario simulation (Fig. 15a/c). The model projects a reduction of up to -2.0 mm for almost all areas of the basin except for the uppermost north showing an increase up to 1.5 mm under the RCP8.5 scenario simulation (Fig. 15b/d).

The mean 95th percentile of daily precipitation intensities during the wet season (Dec.-Feb) is expected to change between -6 mm and 15 mm under the RCP4.5 scenario simulation (Fig. 16b/e), and between -8 mm and 10 mm under the RCP8.5 scenario simulation (Fig. 16c/f) respective to 1971-2000 over the whole Okavango River Basin for the near-future (2016-2045). Under the RCP4.5 scenario simulation, both General Circulation Model (GCM) forcings lead mainly to an increase, but no clear tendency under the RCP8.5 scenario simulation. For the far-future (2071-2100), the projections of the mean 95th percentile of daily precipitation intensity show a change between -8 mm and 10 mm under the RCP4.5 (Fig. 17a/c), and between -8 mm and 15 mm under the RCP8.5 scenario simulation (Fig. 17b/d). Thereby both GCM forcings consistently project an increase over the Okavango River Basin except for the most easterly part under the RCP4.5, and consistently an increase in the Angolan highlands and a reduction in the southeastern part of the basin under the RCP8.5 scenario simulation.

The spatial patterns of the mean frequency of the 95th percentile of daily precipitation intensity are consequently quite similar to the one of the mean 95th percentile of daily precipitation intensity. For the near-future (2016-2045), the mean frequency of the 95th percentile precipitation intensity during the wet season (Dec.-Feb) is expected to change between -1.5 % and 2.0 % under the RCP4.5 (Fig. 18a/c) over the Okavango River Basin respective to 1971-2000. Under the RCP8.5 scenario simulation, the mean frequency of the 95th percentile of daily precipitation intensity shows a change between -2.0 % and 1.5 % (Fig. 18b/d). For the far-future (2071-2100), the simulations project a change in mean frequency of the 95th percentile of daily precipitation intensity of -1.5 % to 2.0 % under the RCP4.5 (Fig. 19a/c), and of -2.5 % to 3.0 % under the RCP8.5 scenario simulation (Fig. 19b/d).

Projections for the mean duration of rainy seasons suggest a change between -50 days and 30 days under both the RCP4.5 (Fig. 20b/e) and the RCP8.5 scenario simulation (Fig. 20c/f) over the whole Okavango River Basin for the near-future (2016-2045). Thereby both scenarios and both GCM forcings indicate consistently a reduction up to 20 days in the Angolan highlands, but no clear tendency in the southern part of the basin (Fig. 20b/e/c/f). Under the RCP8.5 scenario simulation, both model forcings suggest a reduction up to 30 days in the southern Namibian part of the basin (Fig. 20c/f). For the far-future (2071-2100), the mean duration of the rainy season is expected to change between -40 days and 40 days under the RCP4.5 scenario simulation over the whole basin (Fig. 21a/c). Here, both GCM forcings indicate consistently a reduction up to 20 days in the Angolan highlands and the Namibian part of the basin. Under the RCP8.5 scenario simulation, the model projects a change between -50 days and 30 days over the whole basin (Fig. 21b/d). Here, both GCM forcings indicate consistently a reduction up to 30 days in Angolan part as well as a reduction up to 40 days in the Namibian and northern Botswanan part of the basin.

For the near-future (2016-2045), the number of dry spells in rainy seasons is projected to change between -40 and 30 periods under the RCP4.5 (Fig. 22b/e), and between -40 to 20 periods under the RCP8.5 scenario simulation (Fig. 22c/f) over the whole Okavango River Basin respective to 1971-2000. Here, both GCM forcings show opposite change signals. For the far-future (2071-2100), the projections suggest a change in the number of dry spells between -30 and 30 periods under both the RCP4.5 and the RCP8.5 scenario simulation over the whole basin (Fig. 23a-d), thereby both GCM forcings indicate opposite change signals.

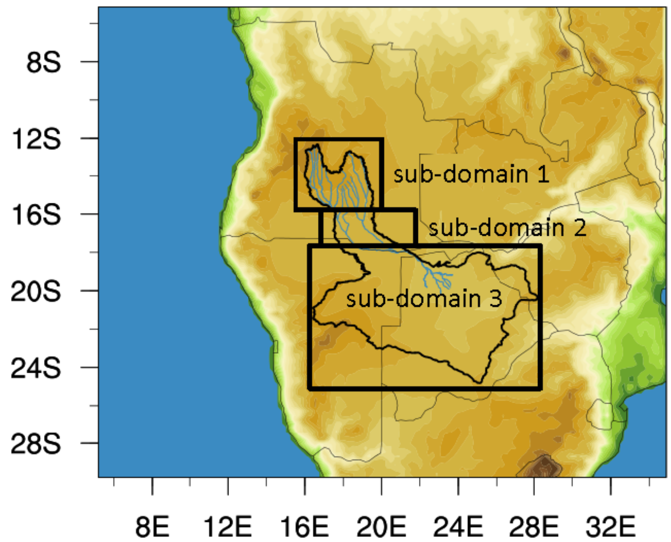

Fig. 1: Okavango River Basin divided into three sub-domains.

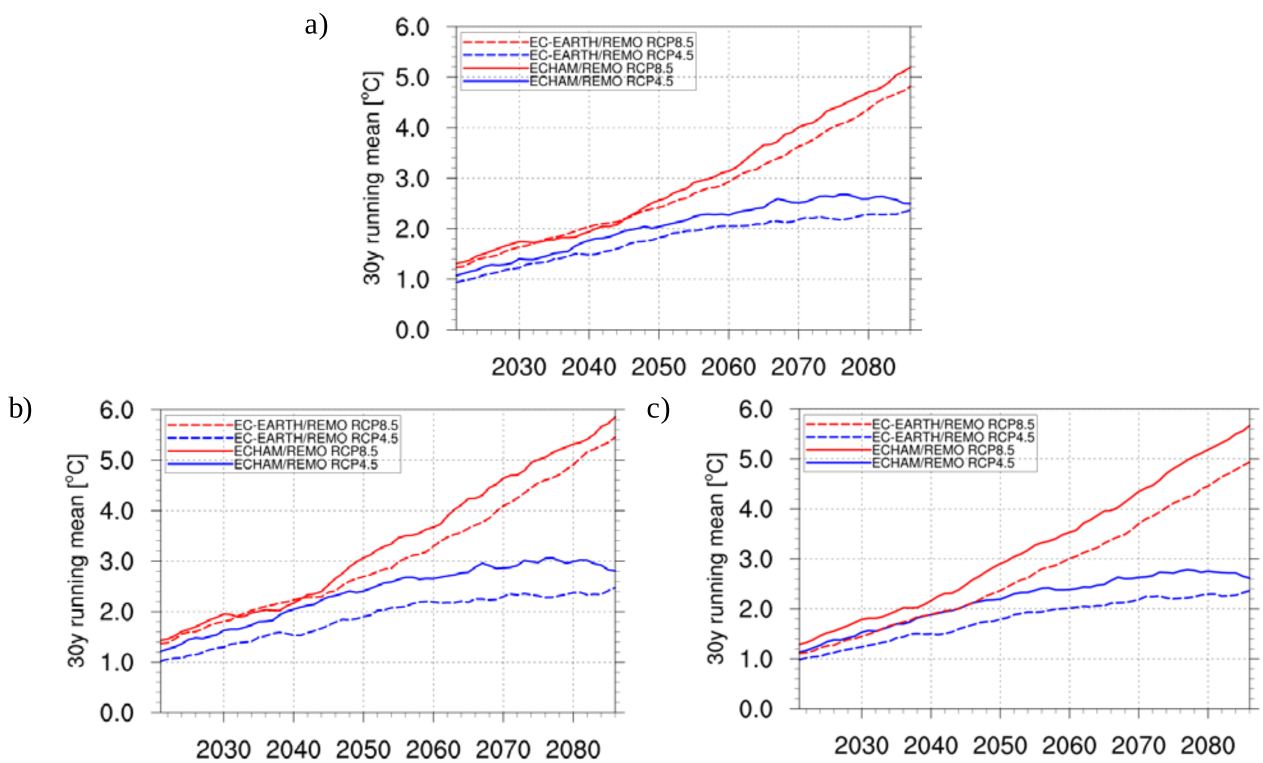

Fig. 2: Projected changes by REMO for annual mean temperature [°C] as spatial average over (a) sub-domain 1, (b) sub-domain 2 and (c) sub-domain 3. Changes are depicted as 30-years running mean for two scenarios (dashed/solid) and two GCM forcings (red/blue) from 2006-2100 respective to 1971-2000.

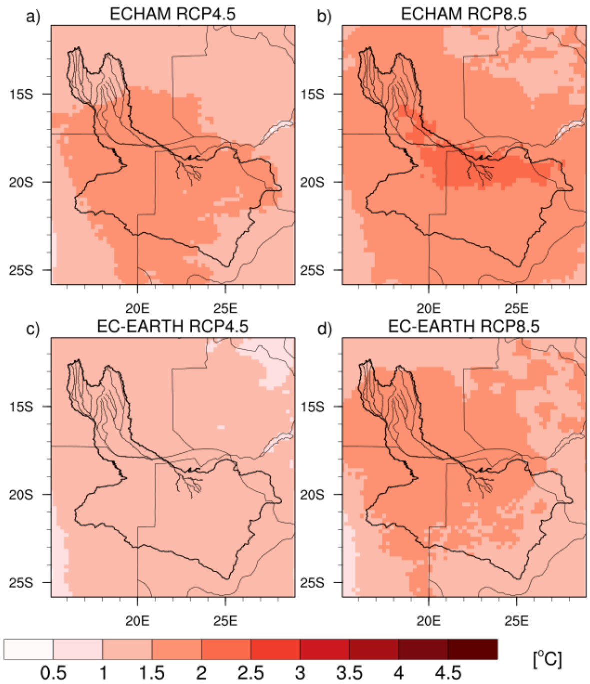

Fig. 3: Projected changes by REMO for annual mean temperature [°C] for 2016-2045 compared to 1971-2000. The upper row shows the ECHAM6 and the bottom row the EC-EARTH forcing. Emission scenarios are represented by different columns.

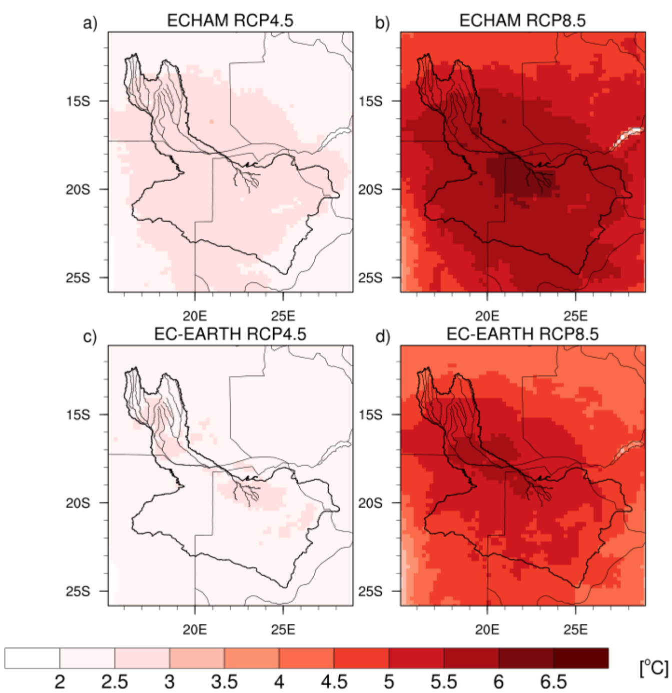

Fig. 4: Projected changes by REMO for annual mean temperature [°C] for 2071-2100 compared to 1971-2000. The upper row shows the ECHAM6 and the bottom row the EC-EARTH forcing. Emission scenarios are represented by different columns.

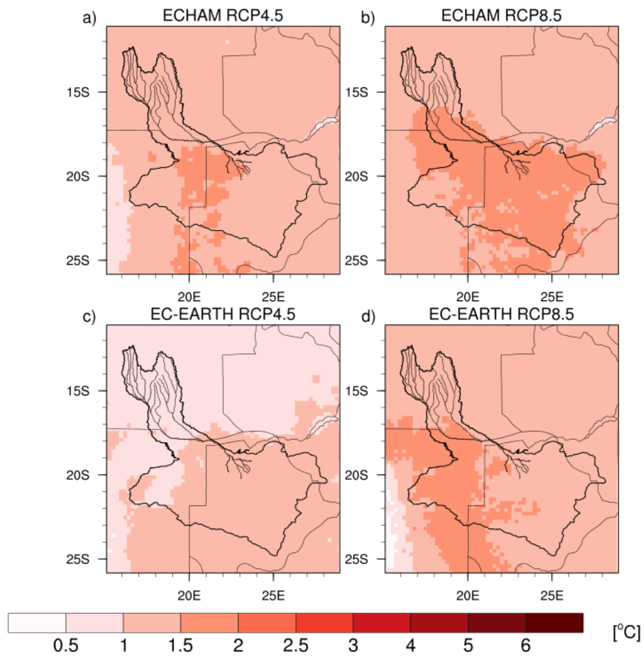

Fig. 5: Projected changes by REMO for Dec.-Feb. mean minimum temperature [°C] for 2016-2045 compared to 1971-2000. The upper row shows the ECHAM6 and the bottom row the EC-EARTH forcing. Emission scenarios are represented by different columns.

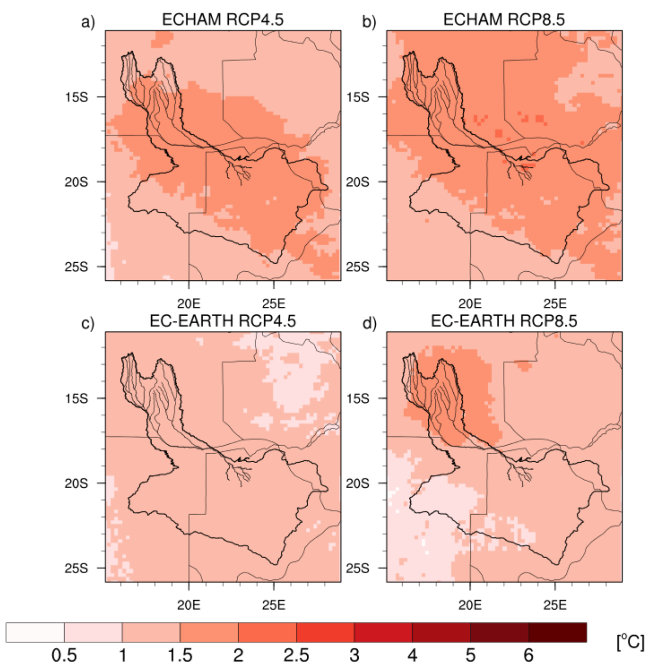

Fig. 6: Projected changes by REMO for Jun.-Aug. mean minimum temperature [°C] for 2016-2045 compared to 1971-2000. The upper row shows the ECHAM6 and the bottom row the EC-EARTH forcing. Emission scenarios are represented by different columns.

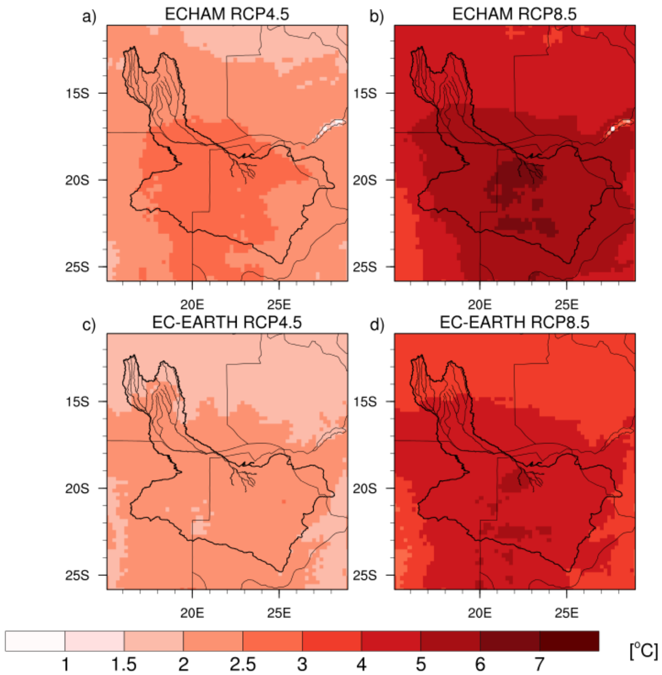

Fig. 7: Projected changes by REMO for Dec.-Feb. mean minimum temperature [°C] for 2071-2100 compared to 1971-2000. The upper row shows the ECHAM6 and the bottom row the EC-EARTH forcing. Emission scenarios are represented by different columns.

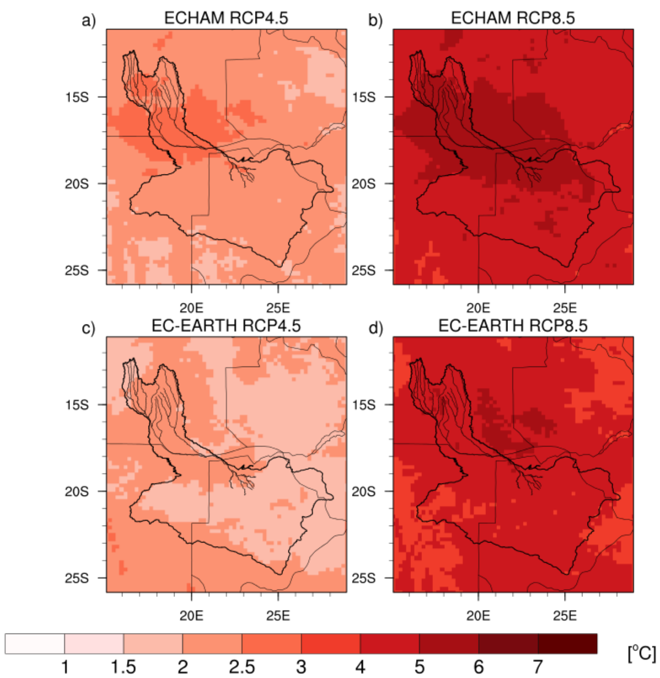

Fig. 8: Projected change by REMO for Jun.-Aug. mean minimum temperature [°C] for 2071-2100 compared to 1971-2000. The upper row shows the ECHAM6 and the bottom row the EC-EARTH forcing. Emission scenarios are represented by different columns.

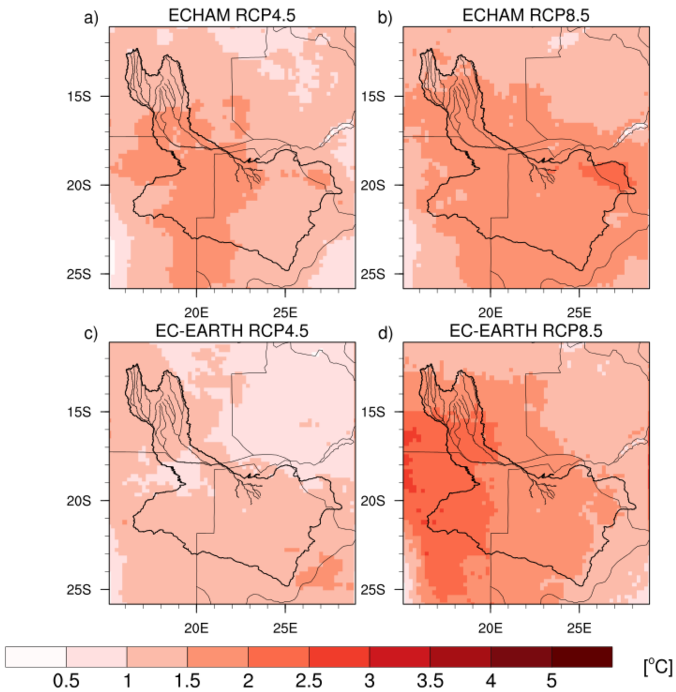

Fig. 9: Projected change by REMO for Dec.-Feb. mean maximum temperature [°C] for 2016-2045 compared to 1971-2000. The upper row shows the ECHAM6 and the bottom row the EC-EARTH forcing. Emission scenarios are represented by different columns.

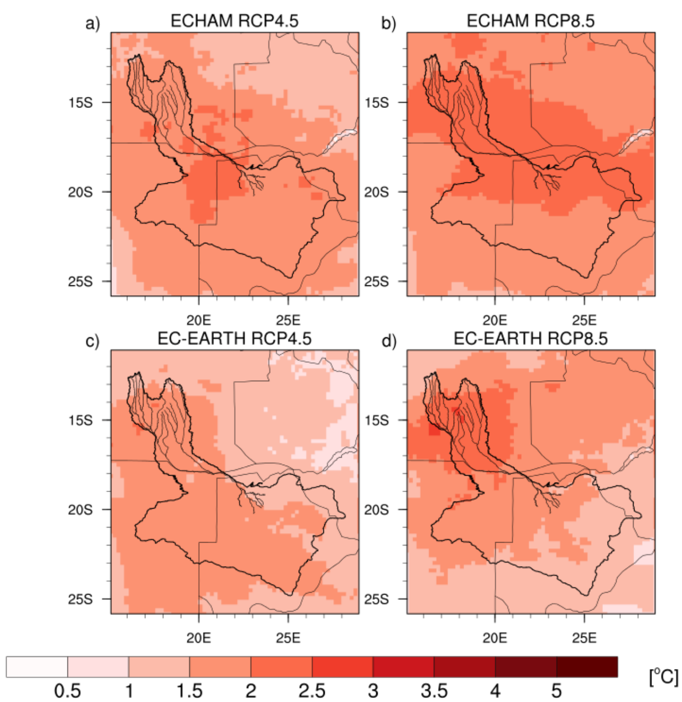

Fig. 10: Projected change by REMO for Jun.-Aug. mean maximum temperature [°C] for 2016-2045 compared to 1971-2000. The upper row shows the ECHAM6 and the bottom row the EC-EARTH forcing. Emission scenarios are represented by different columns.

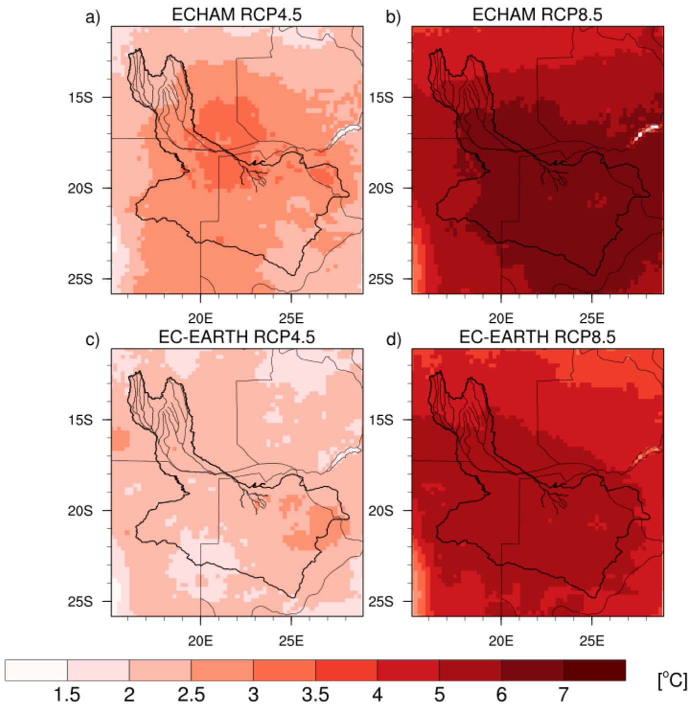

Fig. 11: Projected change in Dec.-Feb. mean maximum temperature [°C] for 2071-2100 compared to 1971-2000. The upper row shows the ECHAM6 and the bottom row the EC-EARTH forcing. Emission scenarios are represented by different columns.

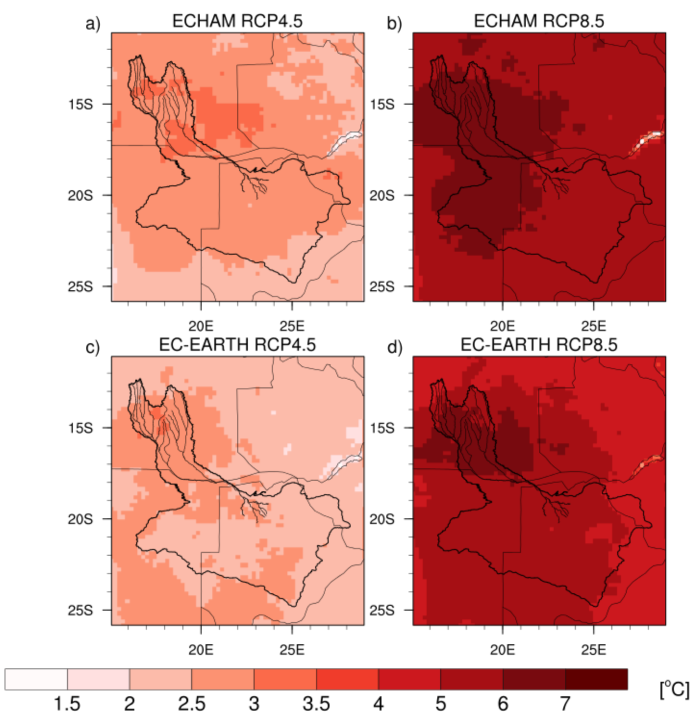

Fig. 12: Projected change by REMO for Jun.-Aug. mean maximum temperature [°C] for 2071-2100 compared to 1971-2000. The upper row shows the ECHAM6 and the bottom row the EC-EARTH forcing. Emission scenarios are represented by different columns.

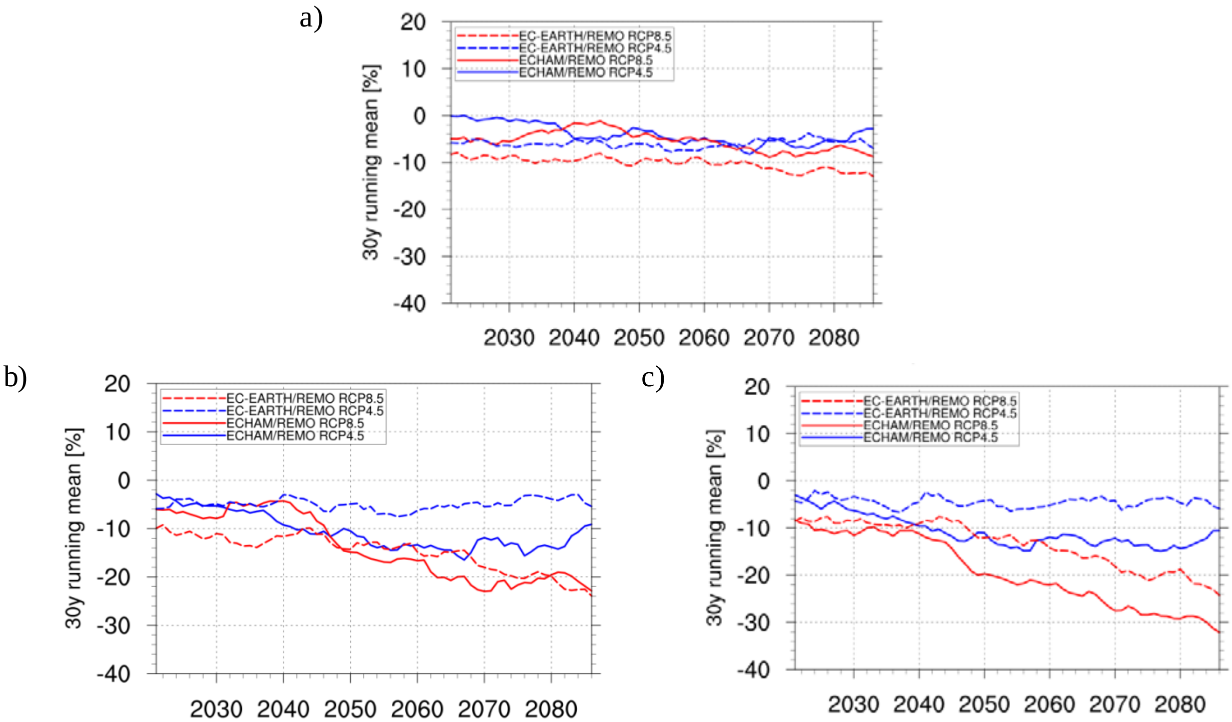

Fig. 13: Projected changes for mean daily precipitation [%] as spatial average over (a) sub-domain 1, (b) sub-domain 2 and (c) sub-domain 3. Changes are depicted as 30-years running mean for two scenarios (dashed/solid) and two GCM forcings (red/blue) from 2006-2100 respective to 1971-2000.

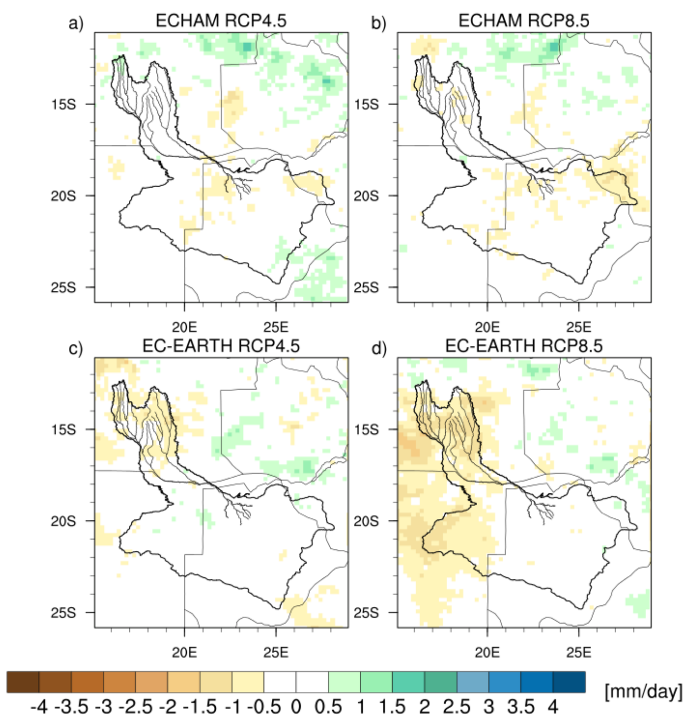

Fig. 14: Projected changes for Dec.-Feb. mean daily precipitation [mm] for 2016-2045 compared to 1971-2000. The upper row shows the ECHAM6 and the bottom row the EC-EARTH forcing. Emission scenarios are represented by different columns.

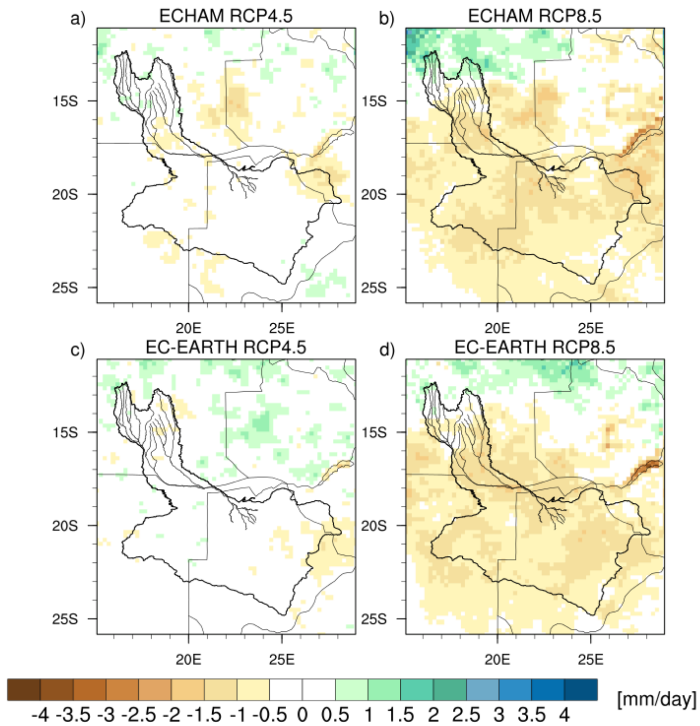

Fig. 15: Projected changes for Dec.-Feb. mean daily precipitation [mm] for 2071-2100 compared to 1971-2000. The upper row shows the ECHAM6 and the bottom row the EC-EARTH forcing. Emission scenarios are represented by different columns.

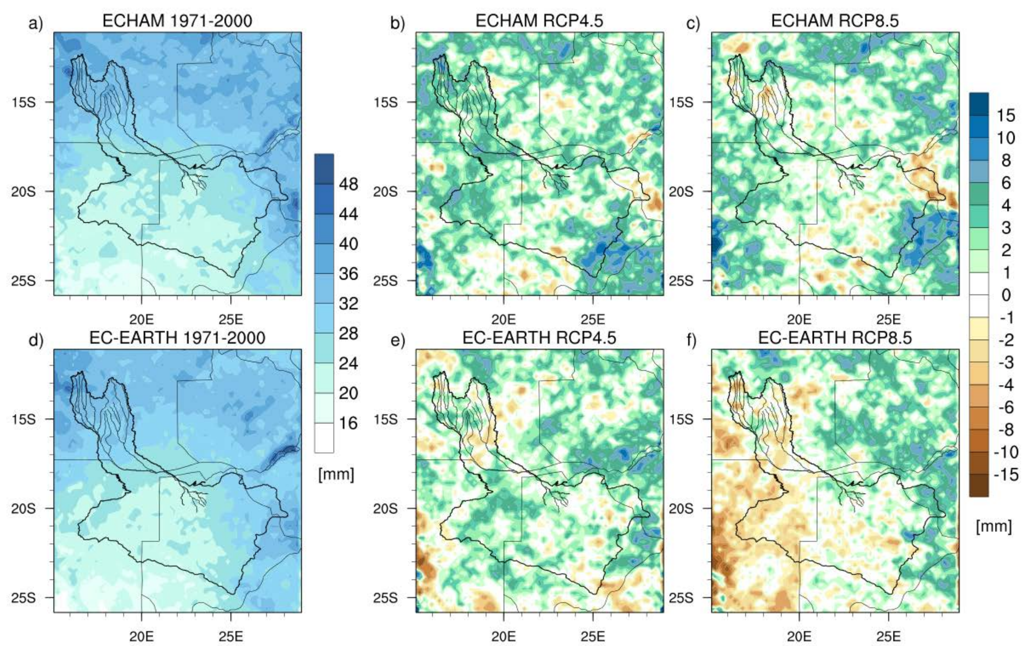

Fig. 16: (b),(c),(e),(f) Projected changes for Dec.-Feb. mean 95th percentile daily precipitation [mm] for 2016-2045 compared to 1971-2000. The upper row shows the ECHAM6 and the bottom row the EC-EARTH forcing. Emission scenarios are represented by different columns.

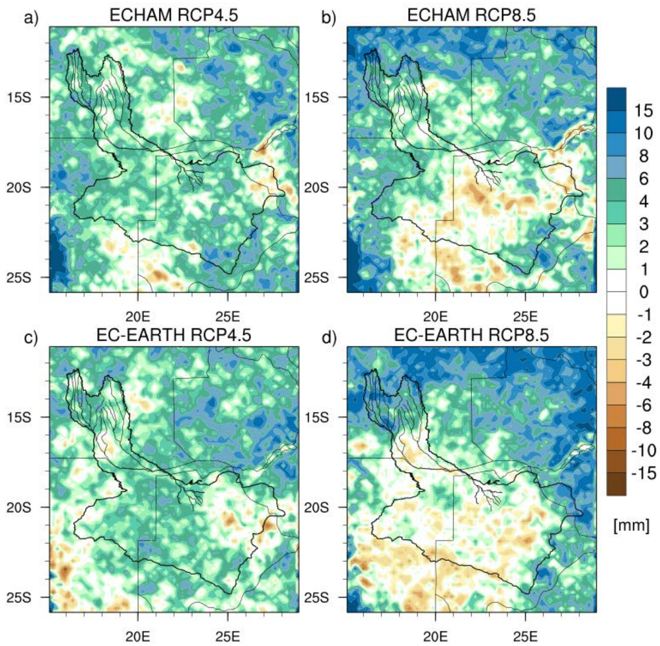

Fig. 17: Projected changes for Dec.-Feb. mean 95th percentile daily precipitation [mm] for 2071-2100 compared to 1971-2000. The upper row shows the ECHAM6 and the bottom row the EC-EARTH forcing. Emission scenarios are represented by different columns.

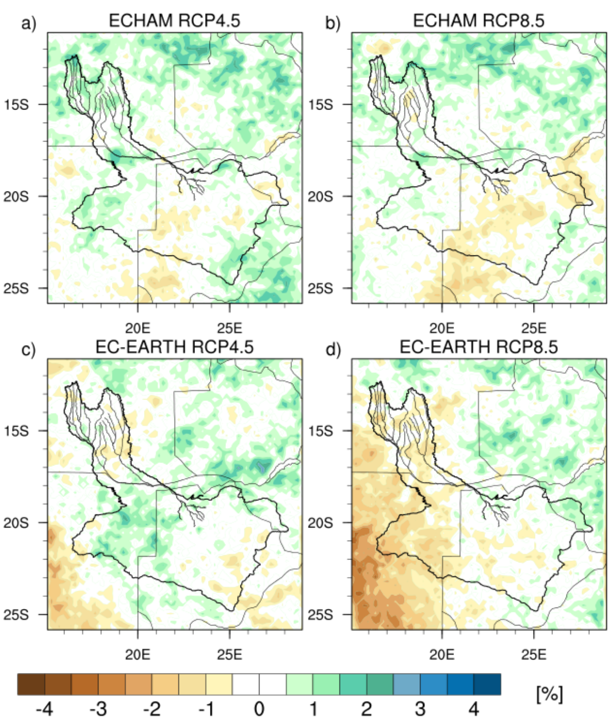

Fig. 18: Projected changes for Dec.-Feb. mean frequency of 95th percentile daily precipitation [%] for 2016-2045 compared to 1971-2000. The upper row shows the ECHAM6 and the bottom row the EC-EARTH forcing. Emission scenarios are represented by different columns.

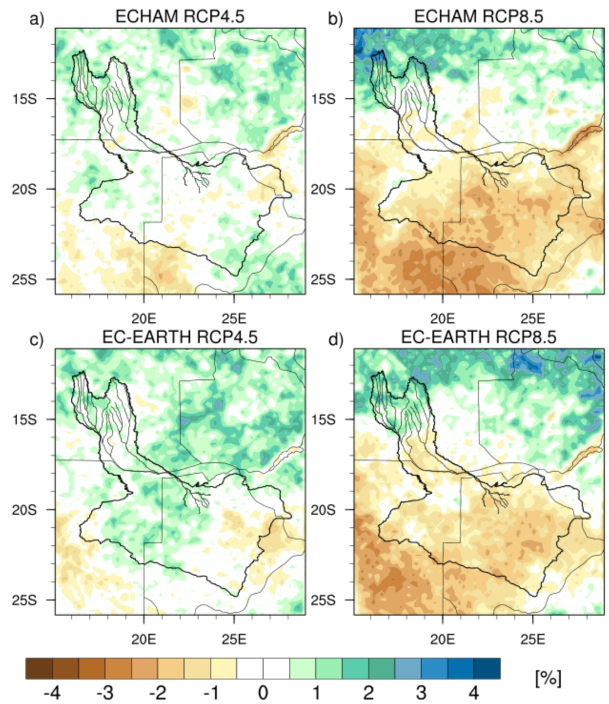

Fig. 19: Projected changes for Dec.-Feb. mean frequency of 95th percentile daily precipitation [%] for 2071-2100 compared to 1971-2000. The upper row shows the ECHAM6 and the bottom row the EC-EARTH forcing. Emission scenarios are represented by different columns.

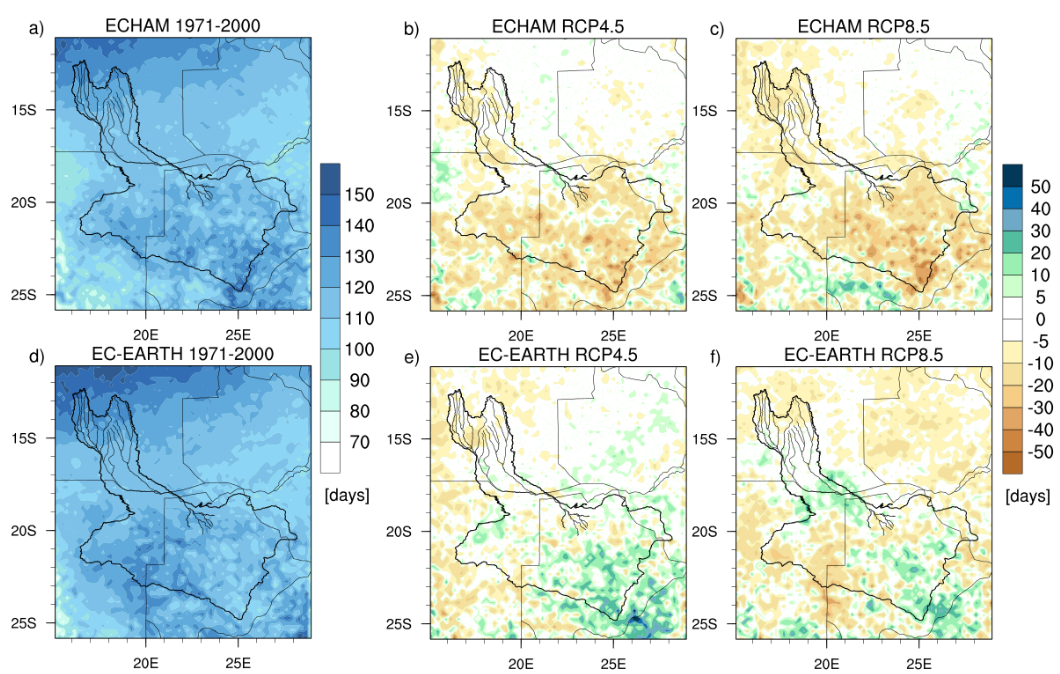

Fig. 20: (b),(c),(e),(f) Projected changes for the duration of the rainy season [days] for 2016-2045 compared to 1971-2000. The upper row shows the ECHAM6 and the bottom row the EC-EARTH forcing. Emission scenarios are represented by different columns.

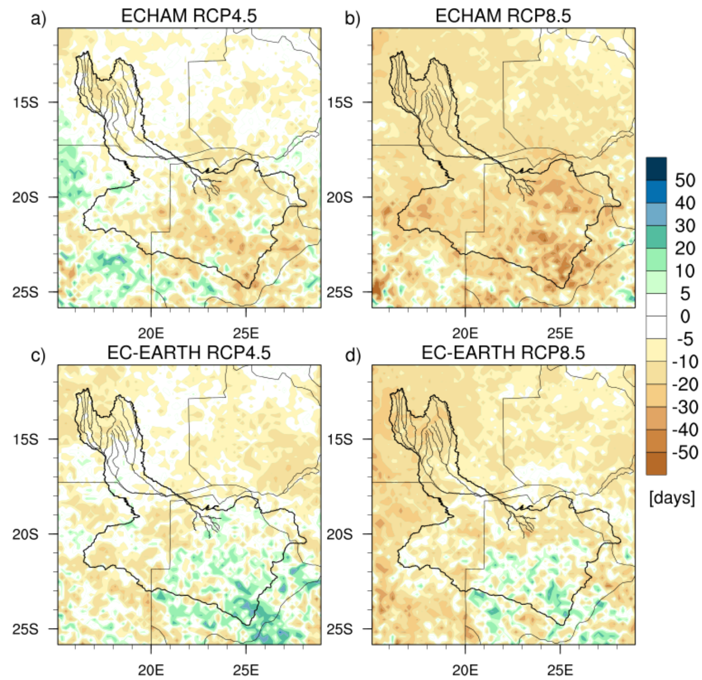

Fig. 21: Projected changes for the duration of the rainy season [days] for 2071-2100 compared to 1971-2000. The upper row shows the ECHAM6 and the bottom row the EC-EARTH forcing. Emission scenarios are represented by different columns.

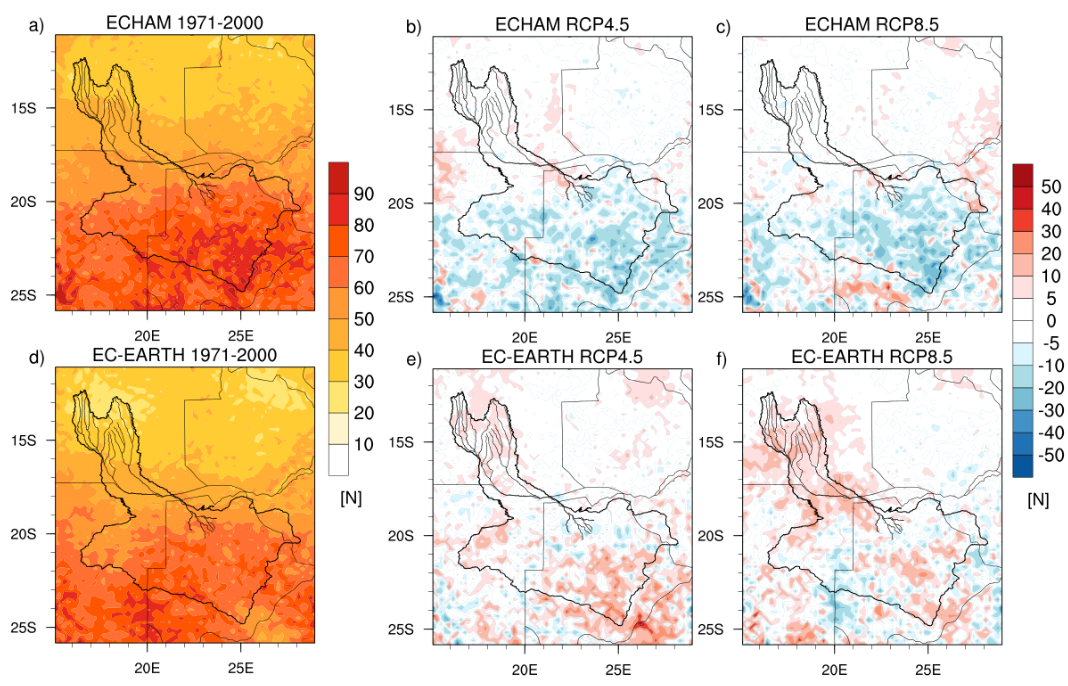

Fig. 22: (b),(c),(e),(f) Projected changes for the sum of dry spells in rainy seasons from 2016-2045 compared to 1971-2000. The upper row shows the ECHAM6 and the bottom row the EC-EARTH forcing. Emission scenarios are represented by different columns.

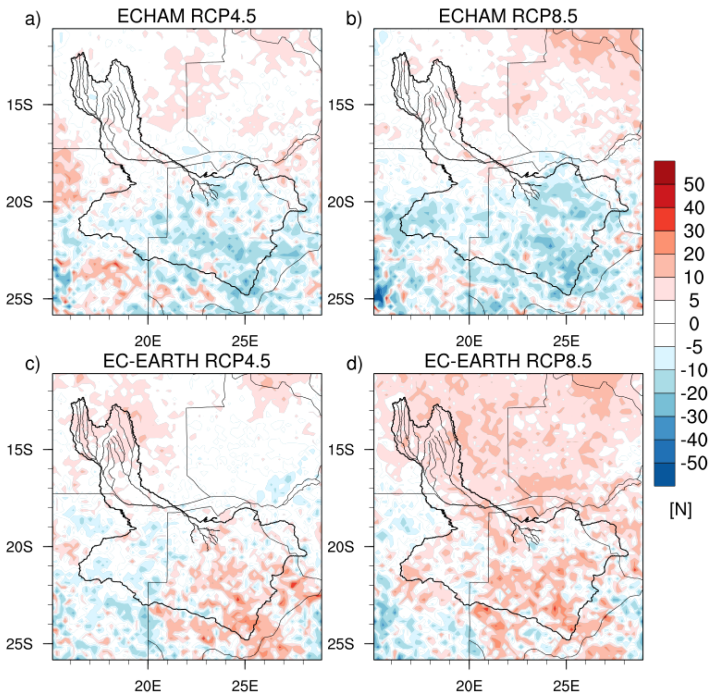

Fig. 23: Projected changes for the sum of dry spells in rainy seasons from 2071-2100 compared to 1971-2000. The upper row shows the ECHAM6 and the bottom row the EC-EARTH forcing. Emission scenarios are represented by different columns.

References

Jacob, D. (2001): The role of water vapour in the atmosphere. A short overview from a climate modeller's point of view. Phys. Chem. Earth A 26 (6–8), 523–527.

Liebmann, B., Blad, I., Kiladis, G. N., Carvalho, L. V., B. Senay, G., Allured, D., Leroux, S. & Funk, C. (2012): Seasonality of African Precipitation from 1996 to 2009. Journal Of Climate, 25(12), 4304-4322, doi:10.1175/JCLI-D-11-00157.1.

Hazeleger, W., Severijns, C., Semmler, T., Ştefănescu, S., Yang, S., Wang, X., Wyser, K., Dutra, E., Baldasano, J. M., Bintanja, R., Bougeault, P., Caballero, R., Ekman, A. M. L., Christensen, J. H., van den Hurk, B., Jimenez, P., Jones, C., Kållberg, P., Koenigk, T., McGrath, R., Miranda, P., Van Noije, T., Palmer, T., Parodi, J. A., Schmith, T., Selten, F., Storelvmo, T., Sterl, A., Tapamo, H., Vancoppenolle, M., Pedro Viterbo, P. & Willén, U. (2010): A Seamless Earth-System Prediction Approach in Action. Bull. Amer. Meteor. Soc. 91, 1357–1363, doi:10.1175/2010BAMS2877.1.

Moss, R.H., Edmonds, J.A., Hibbard, K.A., Manning, M.R., Rose, S.K., van Vuuren, D.P., Carter, T.R., Emori, S., Kainuma, M., Kram, T., Meehl, G.A., Mitchell, J.F.B., Nakicenovic, N., Riahi, K., Smith, S.J., Stouffer, R.J., Thomson, A.M., Weyant, J.P. & Wilbanks, T. J. (2010): The next generation of scenarios for climate change research and assessment. Nature 463, 747–756, doi:10.1038/nature08823.

Stevens, B., Giorgetta, M., Esch, M., Mauritsen, T., Crueger, T., Rast, S., Salzmann, M., Schmidt, H., Bader, J., Block, K. Brokopf, R., Fast, I., Kinne, S., Kornblueh, L., Lohmann, U., Pincus, R., Reichler, T. & Roeckner, E. (2015): Atmospheric component of the MPI-M Earth System Model: ECHAM6. J. Adv. Model. Earth Syst. 5, 146–172, doi:10.1002/jame.20015.